Energy transmission pathways of equatorial waves and associated dissipation process in the Maritime Continent

Yusuke Terada[1], **Yukio Masumoto**[1,2]

[1]Department of Earth and Planetary Science, Graduate School of Science, The University of Tokyo, Tokyo, Japan
[2]Application Laboratory, Japan Agency for Marine-Earth Science and Technology, Yokohama, Japan

Key Points:

- Detailed wave energy pathways within and near the Maritime Continent are identified for the first time with an energy flux analysis
- The Rossby waves from the Pacific Ocean with sufficiently short period induce strong energy dissipation before entering the Indonesian Seas
- A northward energy pathway through the eastern side of the Indonesian Seas appears only for short period waves from the Indian Ocean

Corresponding author: Yusuke Terada, `terada@eps.s.u-tokyo.ac.jp`

Abstract

Detailed pathway of wave energy exchange between the Pacific and Indian Oceans through the Indonesian archipelago and associated energy dissipation are investigated by using a reduced gravity model with realistic coastline. The wave energy flux analysis that can be applicable for all latitudes in a linear shallow water system is adopted. The energy fluxes diagnosed from the model outputs for the incoming Rossby waves from the Pacific clearly indicate two major energy pathways to the Indian Ocean; one turning southward in the Halmahera Sea and reaches the Indian Ocean via the Banda Sea and the Timor Passage, the other passing through the Makassar and Lombok Straits. The former route, however, is shifted to the western side of the island chain within the Banda Sea due to energy trapping around the island chain. It is also found that strong energy dissipation occurs along the northern coast of New Guinea when the period of the incoming Rossby wave is shorter than 1.5 year. In the case of the Kelvin waves from the Indian Ocean, it is found that the major energy pathway is through the Lombok and Makassar Straits to the Pacific Ocean. However, there appears another pathway along the eastern side of the Sulawesi Island in the Banda Sea to exit through the Molucca Sea only when the wave period is shorter than about one month. This secondary pathway makes it easier for the wave energy from the Indian Ocean to reach the western Pacific Ocean for the short period waves.

Plain Language Summary

Indonesian archipelago connects the Pacific and Indian Oceans at low latitude and play a key role in determining regional and global ocean circulations and climate variability by transporting energy and materials. While there are attempts to estimate gross energy transmission of ocean waves through the archipelago from the Pacific to the Indian Ocean and vice versa, detailed pathway of the wave energy within the archipelago and spatial distribution of large energy dissipation associated with the wave propagation have still been veiled. With a new analysis scheme, we identified detailed pathways of wave energy exchange for the first time and their dependencies on the frequency of the incoming wave from both oceans. Two major routes of the energy propagation are determined as a result of complex interplay of planetary waves within the archipelago. In the case of high frequency waves from the equatorial Pacific Ocean, most of their energy dissipate along the northern coast of New Guinea island outside of the archipelago. On the other hand, high frequency waves from the equatorial Indian Ocean are likely to reach the Pacific Ocean because of the existence of an additional pathway through the eastern side of the archipelago.

1 Introduction

The Indonesian throughflow (ITF), driven by the pressure gradient between the Pacific and Indian Oceans (Wyrtki, 1987; Clarke & Liu, 1994), provides a low-latitude pathway of warm and fresh water from the Pacific to the Indian Ocean through the Indonesian archipelago (Gordon, 2005). The ITF constitutes a part of the global thermohaline circulation (Gordon, 1986; Sloyan & Rintoul, 2001), which controls global climate as well as regional and local climate over the Indonesian archipelago. The Indonesian seas also play a role as a wave path connecting the Pacific and the Indian Ocean, by which ocean and climate conditions within the Indonesian archipelago and the surrounding area are affected at various time scales.

Direct observations of the sea level and thermocline temperature variability within the Indonesian archipelago and southeastern Indian Ocean indicate that the interannual variability in these variables are associated with wind forcing in equatorial Pacific, suggesting oceanic wave propagation from the equatorial Pacific to the Indian Ocean through the Indonesian archipelago (Wijffels & Meyers, 2004). Another study by J. Li and Clarke

(2004) using sea level observations also shows penetration of the El Niño signal into the Indonesian archipelago and further into the north and west coast of Australia. Due to the influence of these ocean waves propagating from the Pacific Ocean, the ITF transport and downstream Leeuwin Current show significant variability including the El Nino related signals (Gordon et al., 1999; Feng et al., 2003). It is also suggested that the ocean waves from the Pacific Ocean may generate the Ningaloo Niño events appeared along the northwestern coast of Australia (Kataoka et al., 2014).

The Indonesian archipelago can also be considered as incomplete boundaries of the two basins. Reflection of the equatorial Rossby waves at the entrance of the Indonesian archipelago has been extensively studied as an important process in the delayed action oscillator theory of the El Niño-Southern Oscillation (ENSO) (Suarez & Schopf, 1988). There are several theoretical studies investigating impacts of the reflection of equatorial waves at the leaky Pacific western boundary on the signal reaching the Indian Ocean, which is dynamically associated with the ENSO phenomenon (Clarke, 1991; Du Penhoat & Cane, 1991). In particular, Clarke (1991) assumes the land masses in the western Pacific Ocean and the Indonesian archipelago as thin meridional walls located at representative longitude of each island and suggests that 10% of the energy of the meridional mode 1 Rossby wave coming from the equatorial Pacific penetrates into the Indian Ocean through the Indonesian archipelago at interannual timescales.

To estimate a degree of wave reflection and signal penetration quantitatively with the realistic geometry in the archipelago, reduced gravity models are frequently utilized in several previous studies. Potemra (2001) suggests that energy from the central equatorial Pacific does affect not only the ITF transport but also variability in the southeastern Indian Ocean with significant amplitude at semiannual and longer time scales. Further numerical study by Spall and Pedlosky (2005) shows that 23% of the energy from the equatorial Rossby wave is reflected into the equatorial Kelvin wave at the leaky western boundary of the Pacific Ocean and 10% of the energy reaching the Indian Ocean.

In addition, many studies suggest that significant non-ENSO signals in the ITF transport come from the tropical Indian Ocean (Murtugudde et al., 1998; Qiu et al., 1999; Sprintall et al., 2000; Molcard et al., 2001). For example, Sprintall et al. (2000) observed that a semiannual Kelvin wave, excited in the equatorial Indian Ocean, propagates southeastward along the Sumatra/Java coasts, through the Lombok Strait, and then northward to the Makassar Strait. In addition to the Lombok Strait, the Ombai Strait is also suggested to be an important pathway for the coastally trapped Kelvin waves originated from the equatorial Indian Ocean to flow into the Indonesian archipelago (Durland & Qiu, 2003; Wijffels & Meyers, 2004; Syamsudin et al., 2004). Furthermore, the simple model experiments of Yuan et al. (2018) suggest the possibility of Kelvin wave penetration into the western Pacific from the eastern Indian Ocean through both eastern and western parts of the Indonesian archipelago.

Even if we focus on the horizontal propagation of linear waves, the behavior of the incoming waves with intraseasonal time scale within the Indonesian archipelago is not well understood. Moreover, there is a lack of discussions about where the energy dissipation occurs and how it affects the wave transmission through the archipelago in case of the intrusion of equatorial waves. Therefore, to improve our understanding of processes responsible for the bulk effect of the archipelago, we focus on the incoming waves with a wide range of periodic bands including intraseasonal waves, and the energy dissipation associated with wave propagation.

Recently, Aiki et al. (2017) develops a new analysis scheme of wave energy flux for the planetary waves, which can be applied seamlessly in terms of the latitudinal region. In the present study, therefore, we also examine detailed pathways of wave propagation both from the Pacific to Indian Oceans, and vice versa, by quantitative evaluation based on the wave energy flux of Aiki et al. (2017). For these purposes, a simple reduced grav-

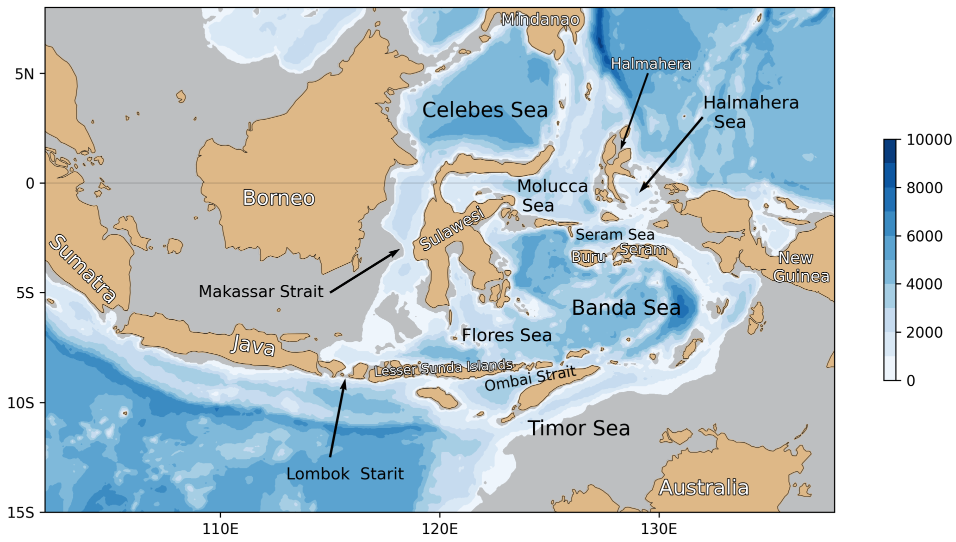

Figure 1. Topography in the Indonesian archipelago. Depths are given in meter. Gray shades indicate areas with depth shallower than 300 meters, which is considered as land masses in the reduced gravity model used in this study.

ity model with realistic representation of the complex geometry of the Indonesian archipelago (Fig. 1) is adopted.

This paper is organized as follows. A numerical model and a method to calculate the wave energy flux are described in Section 2. Section 3 shows results for the cases, in which waves come from the equatorial Pacific Ocean. The wave energy pathways in the Indonesian archipelago and their dependences are discussed. Results for incoming waves from the equatorial Indian Ocean are described in Section 4. Summary and discussion are presented in Section 5.

2 Model and Method

2.1 Numerical Model

We adopt a linear reduced gravity model with one active layer to explore paths of wave energy exchange between the eastern Indian and western Pacific Oceans through the Indonesian archipelago in the simplest possible system. The equations for this model are written as:

$$\frac{\partial u}{\partial t} - yv + \frac{\partial p}{\partial x} = 0$$
$$\frac{\partial v}{\partial t} + yu + \frac{\partial p}{\partial y} = 0$$
$$\frac{\partial p}{\partial t} + \frac{\partial u}{\partial x} + \frac{\partial v}{\partial y} = 0$$

where u and v are zonal and meridional velocities, respectively, η is upper layer thickness anomaly, f is the Coriolis parameter, g' is the reduced gravity and τ_x and τ_y correspond to zonal and meridional wind stress, with $\tau_y = 0$ for all the experiments in this study. The mean thickness of the active upper layer H is set to 300 m, and the coefficient of horizontal viscosity ν has a value of 1×10^{-3} m^2 s^{-1}. The model has a realistic land geometry in and around the Indonesian archipelago based on the contour of 300

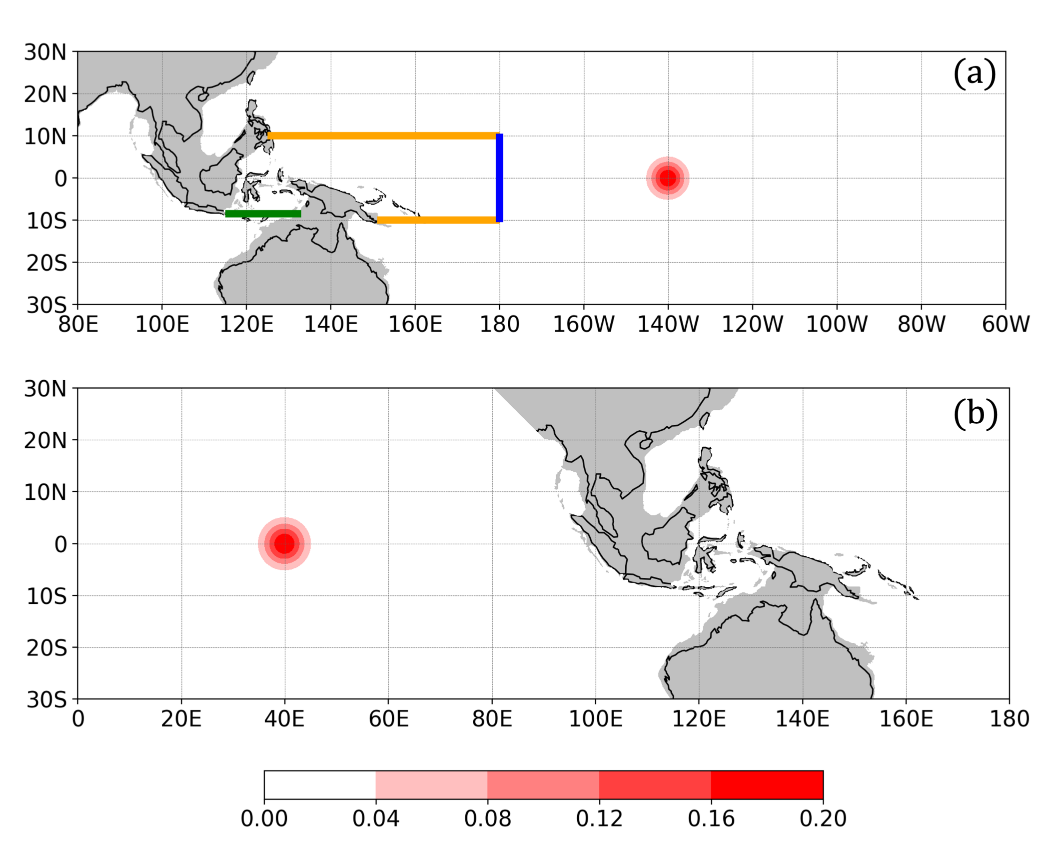

Figure 2. Model domains for (a) the Pacific Ocean experiment and (b) the Indian Ocean experiment, with the amplitude of the idealized zonal wind forcing in N m^{-2} (*color shading*). The model boundaries based on the 300 m isobaths (*gray shade*) are also shown.

m isobath from ETOPO1(Amante & Eakins, 2009), and is forced by idealized zonal winds with a prescribed period of variation. This model is discretized into a spherical coordinate system with a grid spacing of 0.1° in both zonal and meridional directions on the Arakawa-C grid system. At each position of the respective variables, the model integrated the above equations for zonal velocity u, meridional velocity v and upper layer thickness anomaly η. The gravity wave speed $c = \sqrt{g'H}$ was set equal to $c = 2.62$ m s^{-1} as in Potemra (2001), assuming the first baroclinic mode waves in the equatorial Pacific Ocean.

A series of experiments is conducted with two model domains to focus on equatorial waves coming from the equatorial Pacific Ocean or from the equatorial Indian Ocean, respectively. For the Pacific experiment, the model domain extends from 80°E to 60°W and from 30°S to 30°N (Fig. 2a). Sponge layers with the zonal width of 10 degrees for the artificial meridional boundaries at 80°E and 60°W and the meridional width of 5 degrees for the zonal boundaries at 30°S and 30°N are applied along the artificial boundaries to absorb the wave energy and eliminate unexpected reflection and propagation of the waves along the artificial boundaries. Note that results shown below are robust with a wider model domain to include the whole Indian Ocean, since the energy absorption within the sponge layer is quite effective.

Idealized wind forcing for the Pacific experiment is given as

$$\tau_x = A_0 \sin(\omega t) \exp\left[-\left(\frac{x-x_0}{L_x}\right)^2 - \left(\frac{y-y_0}{L_y}\right)^2\right]$$

where (x_0, y_0) is at 140°W on the equator, L_x and L_y are zonal and meridional widths, respectively, with 4 degrees in both directions, A_0 is forcing amplitude of 0.2 N m^{-2}, and ω is the forcing frequency. Since the meridional decay scale L_y is larger than the equatorial deformation radius ($\sim$ 330 km), it is expected that the Rossby wave of the first meridional mode is mainly excited (Spall & Pedlosky, 2005). We apply various forcing period from 90 days to 10 years in this study. The model is integrated for 10 forcing cycles, and the last cycle of the forcing period is used for the following analyses.

The Indian experiment is set similar to the Pacific experiment, but the domain extends from 0° to 180° and from 30°S to 30°N (Fig. 2b). The gravity wave speed c is given as 2.99 m s^{-1} for the first baroclinic mode used in Z. Li and Aiki (2020), and wind stress is applied as

$$\tau_x = A_1 \sin(\omega t) \exp\left[-\left(\frac{x-x_1}{L_x}\right)^2 - \left(\frac{y-y_1}{L_y}\right)^2\right]$$

where (x_1, y_1) is at 40°E on the equator. For the Indian Ocean experiment, we adopt the forcing period from 10 days to 4 years. The other parameters and settings are the same as in the Pacific experiment.

2.2 Analysis Method

Energy flux associated with planetary scale waves is a good indicator for pathways of the wave signals connecting the two basins through the Indonesian archipelago. To obtain wave energy flux in the above numerical model, We utilize a new formulation proposed by Aiki et al. (2017) (hereafter AGC17 scheme), which can be applicable at all latitudes, including the equatorial region, while satisfying coastal boundary conditions. See Appendix for derivation and detailed explanation of the formula. Note that the AGC17 scheme can represent the wave propagation even in the regions where the contribution of viscosity term is large, such as the Indonesian archipelago.

3 Rossby waves from the Pacific to the Indian Oceans

3.1 Energy flux pathways

First, we examine results from experiments with wind forcing in the Pacific Ocean to see the pathways of wave energy transmitted through the Indonesian archipelago. The outputs from the reduced gravity model clearly shows that the wind forcing centering at 140°W excites westward propagating equatorial Rossby waves and eastward propagating equatorial Kelvin waves (Fig. 3a).

The maximum amplitude of the sea level anomaly associated with these equatorial waves is about 5 cm, which is consistent with the satellite observations (Busalacchi et al., 1994; Boulanger & Menkes, 1995; Boulanger & Fu, 1996; Boulanger & Menkès, 1999). Zonal energy flux along the equator clearly shows the eastward propagation of the equatorial Kelvin waves and the westward propagation of the equatorial Rossby waves(Fig. 3b). Meridional distributions of the zonal energy flux across the international date line from the experiments with the forcing of 4-year and semiannual periods are shown in the boxes on the right side of Fig. 4. The meridional structure of the energy flux indicates that almost all incoming waves are meridional mode 1 Rossby waves as expected from the model results of Spall and Pedlosky (2005). Moreover, the horizontal distributions of the wave energy fluxes (left panels in Fig. 4) show the signals penetrating from the

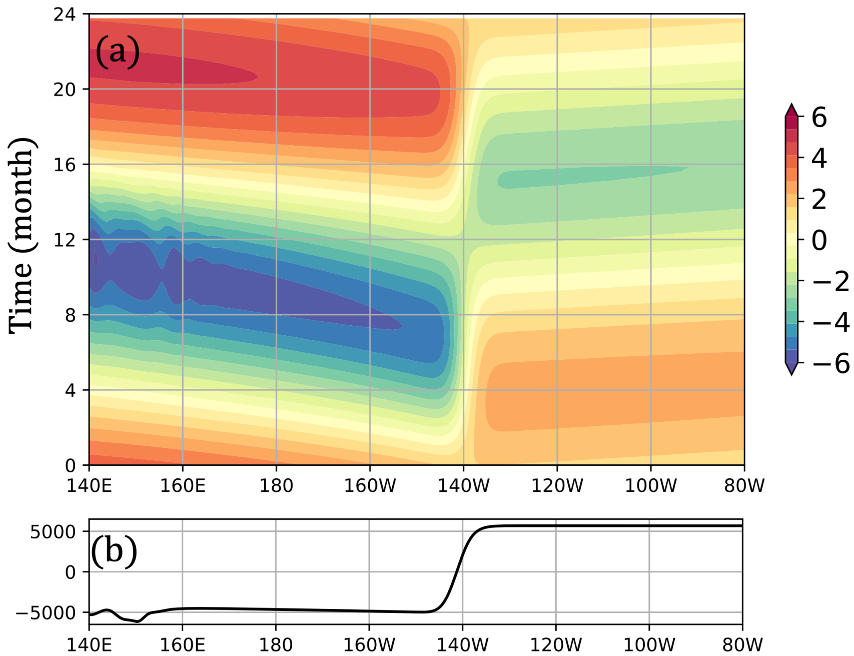

Figure 3. (a) Hovmoller diagram of the sea level anomaly along 2°N for the 2-year period forcing case. The unit is cm. (b) Zonal component of energy flux along the equator for the 2-year period forcing case. The unit is W m^{-1}.

Table 1. Southward energy flux crossing the equator through each passage. Positive value indicates the wave energy flowing into the Indonesian archipelago with a unit of 10^9 W=1 GW.

Period(year)	Makassar St.	Molucca Sea	Halmahera Sea
0.5	0.15	-0.22	0.84
1	0.22	-0.29	0.85
2	0.24	-0.30	0.81
4	0.23	-0.31	0.82

Table 2. Wave energy flux into the Indian Ocean from the Indonesian seas through each passage with a unit of 10^9 W=1 GW.

Period(year)	Lombok St.	Ombai St.	Timor Sea
0.5	0.07	0.05	0.16
1	0.11	0.08	0.14
2	0.12	0.09	0.13
4	0.13	0.09	0.12

Pacific to the Indian Ocean, and then waves continue to propagate southward along the western coast of Australia. The maximum amplitude of the sea level along the western coast of Australia is about 3.5 cm, which is consistent with the observed sea level variations (Clarke & Liu, 1994; Feng et al., 2003). Therefore, the present simple model and its results capture a realistic situation of ocean wave propagation and are worth investigating the detailed processes.

3.1.1 Interannual time-scale

The left panels of Fig. 4 show horizontal distributions of energy flux vectors within and around the Indonesian archipelago, indicating very complex pathways of wave energy from the Pacific to the Indian Oceans for the first time. Note that these vectors only indicate the direction of the energy fluxes and their magnitude is shown in color shades to see the pathways clearly. Table 1 and 2 summarize the energy flux through several key passages at the northern entrance and the southern exit for the archipelago.

In general, for the forcing period of interannual time-scales, most of the wave energy propagates through the Indonesian archipelago within its eastern part; through the Halmahera Sea, the Banda Sea, and the Timor Sea, before reaching the northwestern coast of Australia (Fig. 4a). This eastern route of the wave energy pathway is consistent with the previously mentioned wave pathway suggested from the observed temperature variability and sea level data (e.g. Wijffels & Meyers, 2004). However, there can be seen several notable details in Fig. 4a, which have not mentioned in the previous literatures. One such feature is that the major route of the wave energy occupies the western side of island chain in the eastern Banda Sea. Considering the Kelvin wave propagation along the coasts in the southern hemisphere, major part of the energy flux would be expected through the passage between the Seram and New Guinea Islands. However, most of the energy propagates into the Banda Sea along the west coast of Buru Island and almost no energy propagates along the west coast of New Guinea. We will explore a possible reason for this curious wave energy flux distribution in the following subsection.

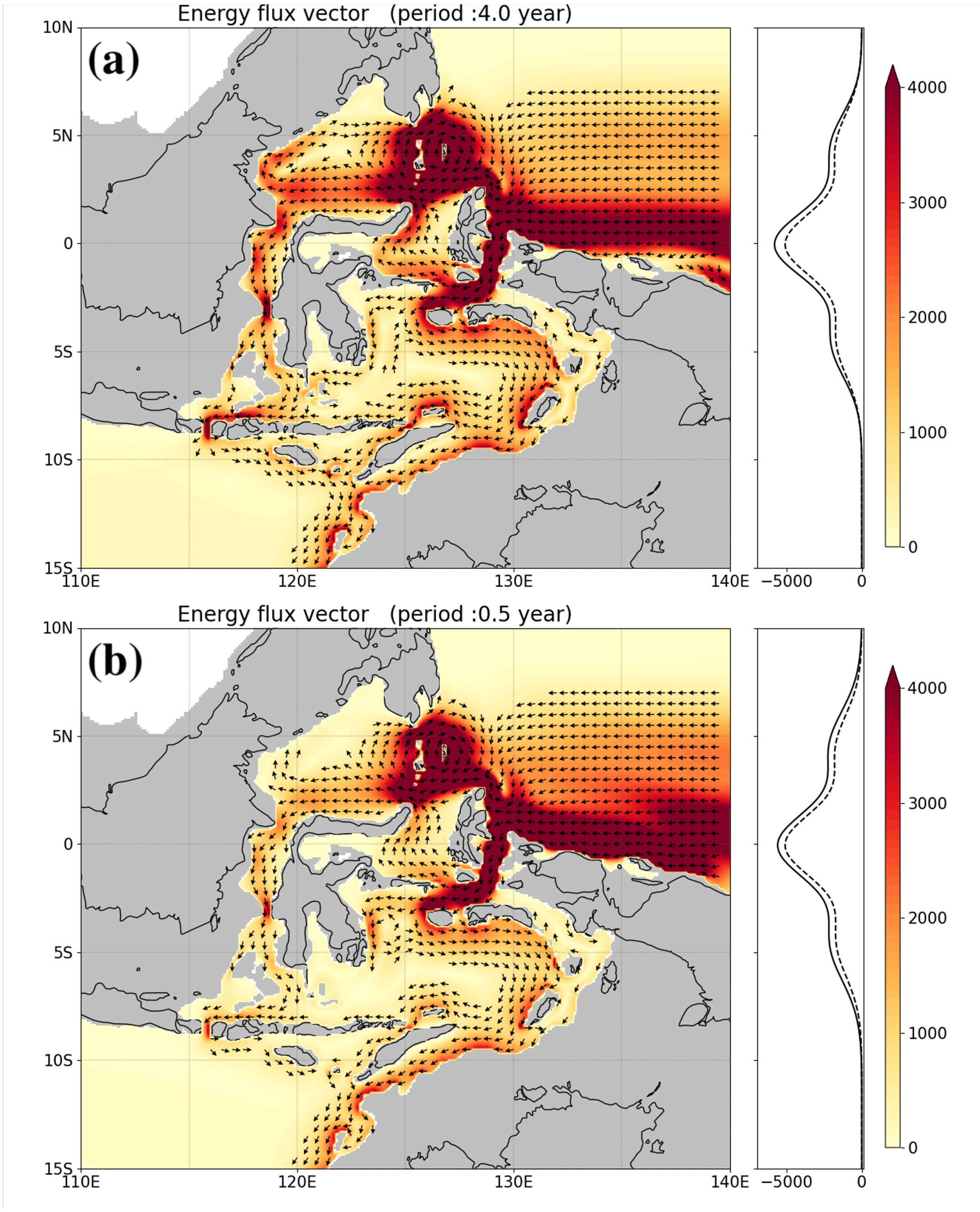

Figure 4. (Left panels) Horizontal distribution of the direction of energy flux vectors (*arrows*) and magnitude of the energy flux in W m^{-1} (*color*). The energy flux vectors are shown only for those with their magnitude larger than 400 W m^{-1}. (Right panels) Meridional distribution of the zonal energy flux of pure incoming wave energy (*solid line*) and analytical values for the first meridional mode 1 Rossby wave (*dashed line*) in W m^{-1}. The forcing period is (a) 4 years and (b) 0.5 years.

After reaching the southern part of the Banda Sea, most of this southward energy flux continue to the Indian Ocean via the Timor Sea. Note that theIn addition, weak southward energy flux appears along the east coast of Sulawesi Island within the Banda Sea from 3°S to 7°S. Note that this poleward energy flux along the east coast of Sulawesi Island is in the opposite direction to the energy propagation due to the coastal Kelvin wave in the southern hemisphere. It is suggested, therefore, that this poleward energy flux is associated with the diffusive boundary layer as mentioned in Spall and Pedlosky (2005). In fact, the width of the southward energy flux along the east coast of Sulawesi Island in the simulated result is about 80 km at 4°S, which is consistent with the representative width of diffusive boundary layer with the viscosity coefficient of 1×10^3 m^2 s^{-1}.

A part of the energy coming to the region south of Halmahera Island returns northward through the Molucca Sea (Table 1), then it merges to the westward energy flux from the northern tip of Halmahera Island to form rather broad westward energy flux to the north of Sulawesi Island. Fig. 4a also shows that about 60% of this wave energy flows into the Makassar Strait and then reaches the Lombok Strait. Besides, the remaining 40% of the wave energy propagates northward along the eastern coast of Borneo Island. This poleward energy propagation is not consistent with the propagation of coastal Kelvin wave, and width of the northward energy flux is about 100 km, suggesting again the energy redistribution in the diffusive boundary layer similar to the eastern coast of Sulawesi Island. It is suggested that not only the wave energy from the Makassar Strait but also the wave energy from the Halmahera Sea and the Banda Sea proceed to the Lombok Strait. Indeed Fig. 4a shows westward energy flux in the Flores Sea, which is due to the Rossby waves off the southern coast of Sulawesi and coastal Kelvin waves along the northern coast of the Lesser Sunda Islands.

Finally, most of the energy propagating southward in the Indonesian archipelago continue to the Indian Ocean mainly via the Timor Sea and Lombok Strait, with the remaining southward energy transfer through the Ombai Strait (Table 2). Although the width of the Ombai Strait is relatively wide compared to the deformation radius at the location of the strait, it is the westward energy fluxes in the Flores Sea that transport a part of energy to the Lombok Strait. Note that the same wave energy pathways as described above are reproduced in experiments with a horizontal viscosity of 1×10^2 m^2 s^{-1}, i.e. ten times larger than the standard case.

In addition, since recent mooring observation suggests that the wave propagation through the Halmahera Sea is not as remarkable as that assumed to be a major waveguide in previous studies (X. Li et al., 2020), the Halmahera Sea in the model of this study may be more favorable to wave transmission due to insufficient resolution ($\sim$ 10 km) to represent many small islands in the Halmahera Sea. However, there is no change in the wave energy pathway in the experiment which applied high horizontal viscosity (5×10^3 m^2 s^{-1}) only in the Halmahera Sea.

3.1.2 Role of Halmahera Island and islands in Banda Sea on the energy pathways

In the previous subsection, the importance of Halmahera Island and islands in Banda Sea on the pathways of wave energy impinging from the equatorial Pacific Ocean is suggested. Here we try to explore their roles in more details with additional experiments removing these islands in the model. In order to clarify the role of Halmahera Island, we first conduct simple experiment only with New Guinea and Australia, without Halmahera Island, and with annual wind forcing as in the main experiments. Fig. 5a shows the energy fluxes in this experiment. It is clearly indicated that most of the incoming energy continues to propagate westward and a small part of the energy propagates along the west coast of New Guinea as coastal Kelvin wave. Slight westward energy fluxes, shown

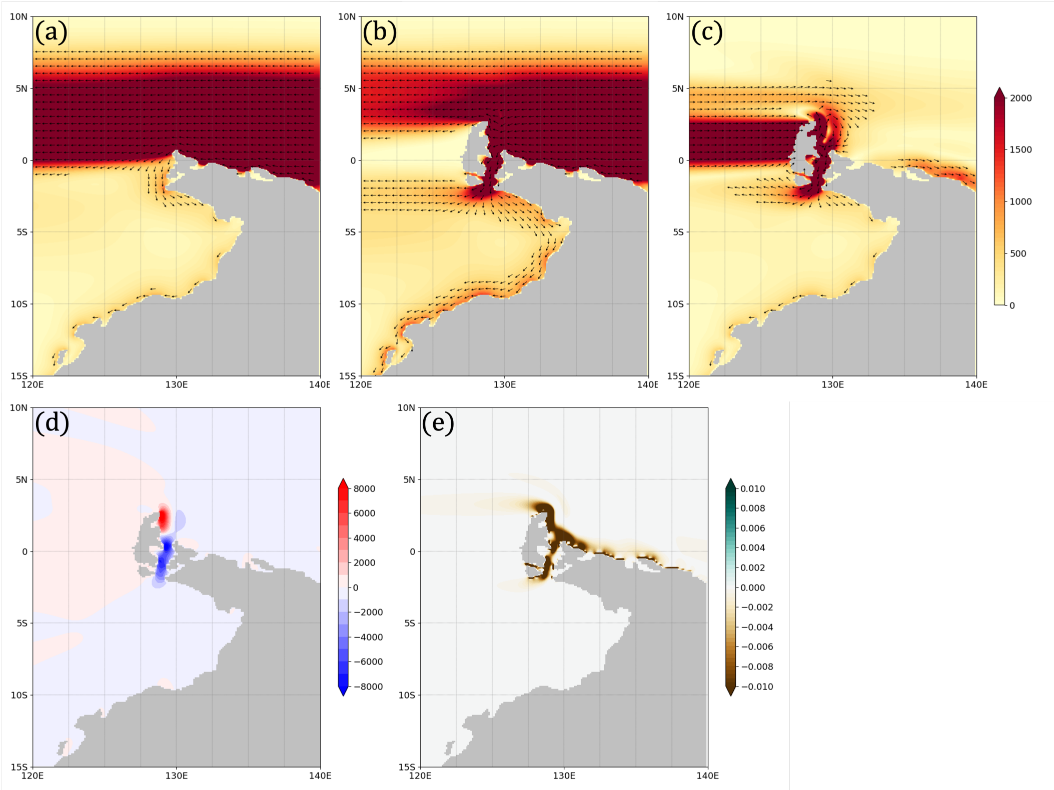

Figure 5. Horizontal distributions of (a) energy flux from a sensitivity experiment only with New Guinea and Australia, (b) energy flux from a sensitivity experiment to which Halmahera Island is added and (c) energy flux differences between the two sensitivity experiments. Arrows indicate energy flux vectors with magnitude larger than 400 W m^{-1} and red color shading indicates magnitude of energy flux in W m^{-1}. (d) Horizontal distribution of the meridional component of energy flux differences in W m^{-1}. (e) Horizontal distribution of the viscous dissipation near Halmahera Island and New Guinea for with Halmahera case in W m^{-1}.

as light color shades without arrows, corresponding to Rossby wave emitted from the coastal Kelvin wave can also be seen on the western side of New Guinea and Australia.

As a second step, Halmahera Island is added to the experiment (Fig. 5b). The difference in the energy flux between the two experiments (Fig. 5c,d) can be considered as the contribution of Halmahera Island to the wave energy propagation. Fig. 5c clearly shows that the Halmahera Island has a barrier effect on the westward equatorial Rossby wave, and the blocked Rossby wave energy continues to propagate southward through the Halmahera Sea, resulting in enhancement of the Rossby waves in southern hemisphere and the southward coastal Kelvin wave. Fig. 5d shows strong southward and northward energy fluxes in the Halmahera Sea, and strong energy dissipation along the eastern coast of the Halmahera Island is shown in Fig. 5e. All these results suggest the importance of the diffusive boundary layer to the wave energy propagation.

To investigate the reasons why the wave energy does not propagate along the west coast of New Guinea as shown in Fig. 4, we conducted an additional sensitivity experiment with Buru and Seram Islands and the island chain in the eastern Banda Sea. Fig. 6 shows the contribution of these islands to the energy transport. The island chain has only a small effect on wave energy to reflect back to the Pacific Ocean, and most of the

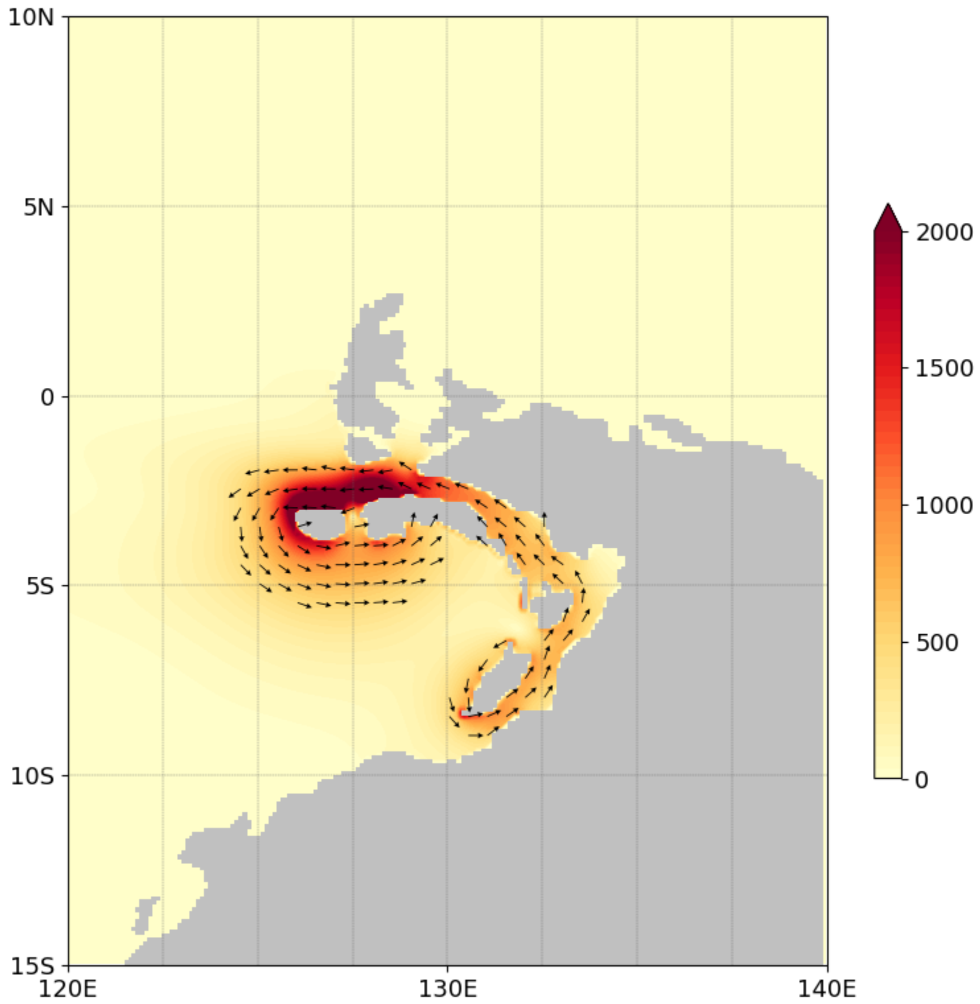

Figure 6. Same as Fig. 5c but for the energy flux differences between experiments with and without Buru and Seram Islands and the island chain in the eastern Banda Sea. (with island chain case minus no island chain case)

wave energy flows into the Indian Ocean as in the case with Halmahera Island (Fig. 5b). In addition, an anticlockwise energy circulation around the island chain is clearly seen in Fig. 6, which is superposed on the southward energy flux along the west coast of New Guinea in the case with Halmahera Island, providing almost no energy flux in the total fields. Thus, the absence of the easternmost energy path can be attributed to the cancellation of Kelvin wave along the west coast of New Guinea by the energy circulation trapped around the islands in the Banda Sea. It takes only about 10 days for Kelvin waves to bypass the islands of the Banda Sea and develop the energy circulation with the group velocity of the first baroclinic mode coastal Kelvin wave (~ 2.6 m s^{-1}), suggesting that it is difficult to detect signals that has a period longer than 10 days from the Pacific Ocean using mooring observations on the west coast of New Guinea.

3.1.3 Semiannual time-scale

The energy pathways shown for the incident waves of different interannual time scales (2- to 10-year period) are very similar to those obtained for the 4-year period case discussed above. The approach taken in this study, numerical experiments with realistic boundaries and AGC17 scheme, also enables us to investigate the energy propagation of higher frequency waves, which has not been discussed much in the previous literatures. It is important to evaluate energy pathways for such shorter time-scale variations since the semiannual variations are observed in the western tropical Pacific (e.g. Qu et al., 2008). In addition, atmospheric intraseasonal oscillations, such as the Madden-Julian oscillation (Madden & Julian, 1994), can generate equatorial Kelvin and Rossby waves through surface zonal winds over the Pacific Ocean (Hendon et al., 1998; Zhang et al., 2001) and may affects the Indonesian archipelago.

The results of semi-annual forcing case (Fig. 4b) also show two major energy pathways; one through Halmahera Sea and Banda Sea and the other through Makassar Strait and Lombok Strait as in the case of low frequencies. However, the magnitude of the energy flux is clearly smaller than that of the low frequency case. In particular, the decrease in magnitude is significant in the pathway through the Makassar Strait and Lombok Strait (see Table 2). This discrepancy is attributed to the difference in the amount of energy dissipation at the western boundary of the Pacific Ocean, which is discussed in the next subsection on the energy budget. The decrease in the energy flux through the Lombok Strait may also be due to the reduction of the westward propagating Rossby wave in the Flores and Banda Seas at high frequencies.

3.2 Energy budget

3.2.1 Energy budget for a larger domain

To evaluate the energy budget in a larger domain, a box covering the western equatorial Pacific and the Indonesian archipelago is considered (Fig. 2a) and the amount of wave energy crossing the boundaries is calculated (Fig. 7). It should be noted here that wave energy flux across the eastern section at 180°E averaged over one forcing period, E'_{in} includes both the incoming wave energy flux and the flux due to reflected waves. In order to extract pure incoming wave energy crossing the international date line, we conducted an additional experiment, in which a simple meridional western boundary with a sponge layer is incorporated to erase the wave energy associated with the reflected equatorial Kelvin wave. The energy flux across the international date line for this experiment can be considered as the pure westward incoming wave energy, E_{in}, and therefore eastward reflected wave energy, E_{ref}, can be defined as

$$E_{\text{ref}} = E_{\text{in}} - E'_{\text{in}}$$

Fig. 7 shows results of the energy budget as a function of the forcing period, standardized by the incoming energy across the date line for each forcing period. It is clearly shown that, for the period longer than 1.5 years, most of the incoming energy (about 60%) is dissipated within the box, while about 30% of the incoming energy is reflected back to the east of the date line. Then, the remaining 10% of the incoming energy flows into the Indian Ocean. Since the wind forcing in our experiment excites the meridional mode 1 equatorial Rossby wave (see Fig. 4), this result is in good agreement with the result of the analytical investigation by Clarke (1991) and the model calculations by Spall and Pedlosky (2005).

Horizontal distributions of energy dissipation rate are shown in Fig. 8. Comparing high frequency and low frequency cases, there is a common feature that strong energy dissipation occurs in the western boundary layer regions of the Pacific Ocean, such as zonally narrow regions off the east coast of Mindanao, Borneo, Halmahera and New

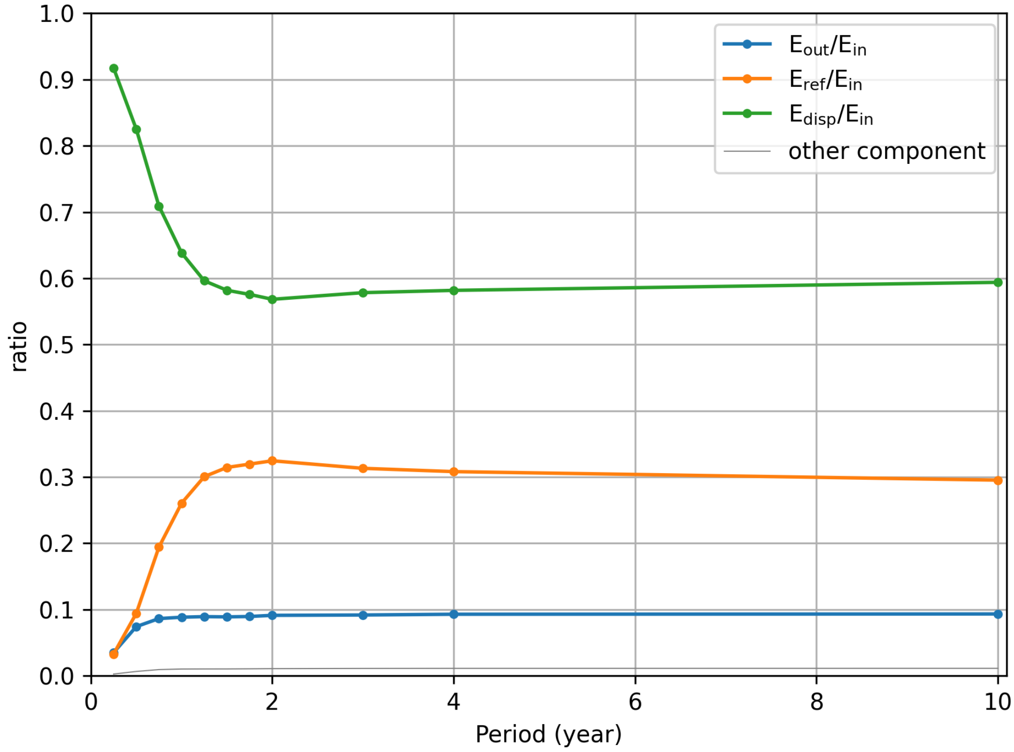

Figure 7. Ratios of major terms in the wave energy budget in the box shown in Fig. 2a to the pure incoming wave energy flux across the international date line.

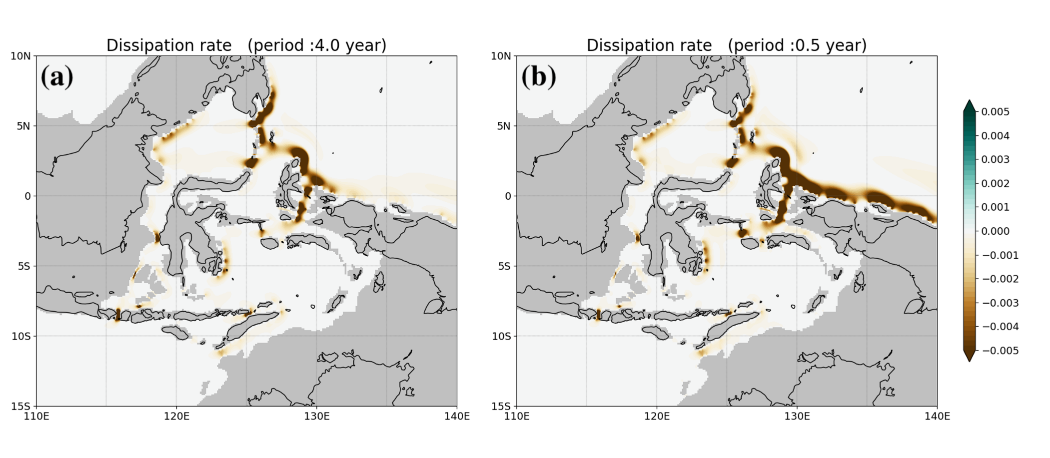

Figure 8. Horizontal distribution of dissipation rate obtained from experiments with the wind forcing of (a) 4 year and (b) 180 day periods. The unit is W m^{-2}.

Guinea, as well as regions within the narrow channel such as the Halmahera Sea and the northern entrance of the Banda Sea. In addition, there is strong energy dissipation in the northern coast of Buru Island, as well as the narrow part of the Makassar Strait and the Lombok Strait. Note that northward and southward leakage of the energy across 10°N and 10°S are almost negligible for all frequencies.

For the forcing period less than 1.5 years, unlike the low frequency case, the ratio of dissipated energy within the box increases and that of reflected energy decreases as the period becomes shorter (Fig. 7). This tendency is consistent with the result of Spall and Pedlosky (2005), but their result only shows the decreases of dissipated and transmitted energy qualitatively. Thus, detailed quantitative understanding of why the reflection and the transmission are suppressed at higher frequency is necessary. In the high frequency case (Fig. 8b), the dissipation rate is significantly large along the northern coast of New Guinea between 130°E and 140°E, which cannot be seen in the low frequency case (Fig. 8a). The forcing period of 1.5-year seems to provide a key time-scale for setting up two regimes; one with the weaker dissipation along the northern coast of New Guinea (i.e. the low-frequency cases) and the other with the stronger dissipation there (i.e. the high-frequency cases). It is worth noting that the 1.5-year corresponds to a wave period, for which half of the zonal wavelength of the incoming meridional mode 1 Rossby wave is comparable to the zonal width of the inclined western boundary (New Guinea Island) in the present case. We will discuss a possible mechanism responsible for this difference in the dissipation magnitude in detail in the next subsection.

3.2.2 Dissipation along the northern coast of New Guinea

In the previous studies of the reflection of the equatorial Rossby waves at inclined western boundary (e.g. Cane & Gent, 1984; McCalpin, 1987), the reflection at the western boundary is considered from the budget of mass flux across the boundary between the western boundary layer and the interior ocean, and remaining energy is treated to be dissipated in the western boundary layer. However, since we consider the energy penetration further to the west, we need to examine the energy dissipation on the inclined western boundary in detail.

To evaluate the energy dissipation on the western boundary in a simpler case, experiments without Solomon Islands and New Ireland are conducted. In these additional

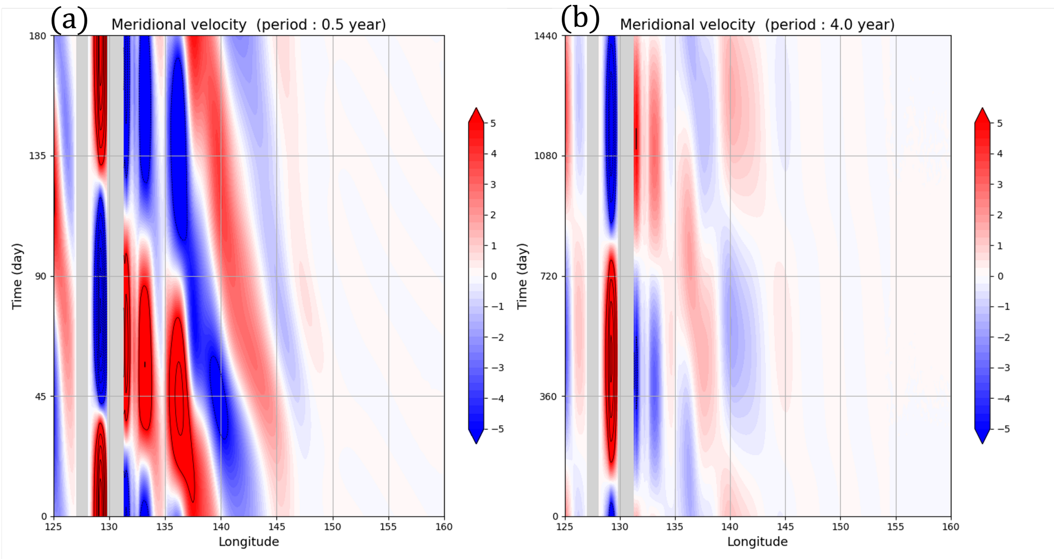

Figure 9. Hovmoller diagrams of the meridional current along the equator for (a) the 4-year period forcing case and (b) the semi-annual forcing case in cm s^{-1}. Contours indicate meridional velocity with amplitudes above 5 cm s^{-1} and contour intervals are 5 cm s^{-1}.

experiments, energy transmission and reflection rates show the same dependencies on the forcing period as in the main experiments (Fig. 7). Furthermore, strong energy dissipation along the northern coast of New Guinea can be seen only when forcing period is shorter than 1.5 years. Fig. 9 shows time evolutions of meridional currents along the equator when the forcing periods are 4 years and 0.5 years. In both cases, the meridional velocity is significant in the region near the western boundary of the Pacific Ocean (130-145°E). However, the amplitudes of the meridional velocity show very different values: it is about 2 cm s^{-1} for the 4-year period case while it becomes well over 5 cm s^{-1} for the 0.5-year period case.

To clarify the processes that generate the meridional currents across the equator with different amplitude for the short-period and long-period cases, we consider the mass flux entering the inclined west boundary layer as in Cane and Gent (1984); McCalpin (1987). When the forcing period is long enough (the zonal wavelength of the incoming Rossby waves is sufficiently longer than the zonal extent of the inclined western boundary), incoming Rossby waves reach the western boundary layer at almost the same phase at any latitude, and the meridionally symmetric mass fluxes enter the west boundary layer. In this case, most of the off-equatorial incoming mass fluxes of the Rossby waves generate equatorward currents in the western boundary layer for redistributing the masses toward the equator and emitting them eastward as the equatorial Kelvin waves. The direction of the mass redistribution in the western boundary layer is opposite in the northern and southern hemispheres, thus meridional current across the equator is less likely to be formed (Fig. 9a). On the other hand, when the forcing period is rather short, i.e. the zonal wavelength of the incoming Rossby waves is comparable to or less than the zonal extent of the inclined western boundary, incoming Rossby waves reach the western boundary layer at different phases at each latitude, and the meridionally asymmetric mass fluxes are generated in the west boundary layer. For example, a positive mass flux enters in the southern hemisphere while a negative mass flux enters in the northern hemisphere. In this case, the total mass flux entering the western boundary layer, capable of constructing the reflected Kelvin waves, is very small. Therefore, strong meridional current across the equator is formed to connect the asymmetric mass distribution in the western boundary layer (Fig. 9b). This strong current across the equator and in the western boundary layer generates large horizontal velocity shier, inducing the strong energy dissipation particularly along the northern coast of New Guinea (Fig. 8b).

Since both the incoming meridional mode 1 Rossby waves and the reflected equatorial Kelvin waves have no meridional velocity at the equator, the meridional currents shown in Fig 9 suggest the existence of the other type of waves. In fact, Fig. 9 indicates the westward phase speed of about 10 cm s^{-1} with the eastward group velocity of about 50 cm s^{-1} between 140°E and 150°E, and this group velocity correspond to that of the Yanai waves with a period of about 20 days. The existence of the Yanai waves is also confirmed in Fig. 10, which shows the zonal distribution of the time averaged meridional velocity for the gravest four modes of the equatorial Rossby waves and the Yanai wave. When incident Rossby wave approaches the inclined western boundary, the meridionally asymmetric mode Rossby waves and the Yanai waves are excited to satisfy the boundary condition. Since these reflected waves have a group velocity smaller than the incoming meridional mode 1 Rossby waves, they are superposed on the incoming waves with the out-of-phase relation. Since the New Guinea coast extends far eastward to 150°E, the superposition of the waves create a strong horizontal shear of the along shore current fields that efficiently dissipates wave energy. The proportion of time with strong horizontal current shear to one period of the incident Rossby wave becomes longer as the wavelength of the incident wave becomes shorter. Therefore, more energy is dissipated in the western boundary layer along the northern boundary of New Guinea when incoming wave period is shorter.

4 Kelvin Waves From the Indian to the Pacific Oceans

4.1 Responses within the Indian Ocean

For the Indian Ocean experiment, we consider whether and how the equatorial Kelvin waves propagate through the Indonesian archipelago and eventually penetrate into the Pacific Ocean. We first investigate briefly the behavior of waves before they reach the Indonesian archipelago. For a period shorter than 30.7 days, below which no equatorial Rossby waves satisfy the dispersion relation under our model settings, most of the wave energy propagates southeastward along the coast of Sumatra Island after reaching the eastern boundary of the Indian Ocean (Fig. 11a). Only a small part of the incoming wave energy propagates to the north into the Andaman Sea along the eastern boundary of the basin.

On the other hand, for the Kelvin waves with longer periods, the wave energy bifurcates northward and southward off Sumatra Island. While most of the energy reflects westward as Rossby waves and propagates along the coast of the Bay of Bengal in the northern hemisphere, they are divided into westward Rossby waves and eastward coastal Kelvin waves in the southern hemisphere (Fig. 11b). Fig. 11c shows northward energy fluxes across 4° and 12° latitude sections near the eastern boundary in both hemispheres as a function of the forcing period. The results indicate that more than a half of the energy crossing 4°N reaches 12°N and propagate further north into the Bay of Bengal while the energy reaching 12°S is almost zero. This north-south difference suggests that the Bay of Bengal is more sensitive to equatorial waves originating from the equatorial Indian Ocean than the Southeastern Indian Ocean.

Fig. 11c also shows dependences of energy flux magnitude on the forcing period. While the wave energy across 4°N or 4°S is evenly distributed for the longer periods, we can find asymmetric energy partition between the two hemispheres for sufficiently short period, with more energy in the southern hemisphere. In addition, northward wave en-

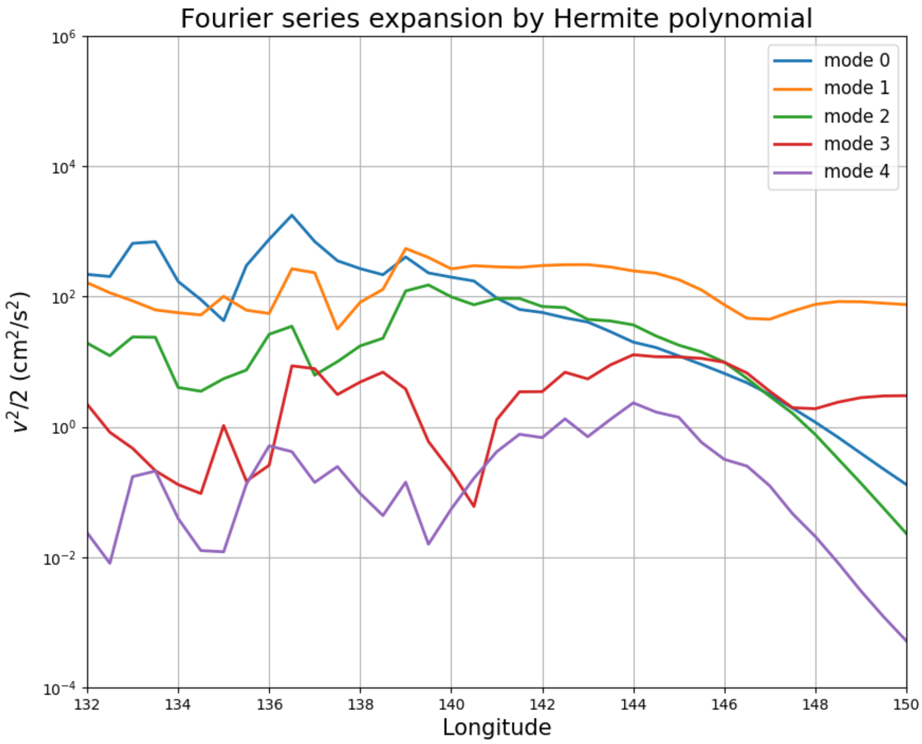

Figure 10. Time averaged amplitude of $v^2/2$ for each meridional mode of the equatorial waves for the semi-annual forcing case (Fourier series expansion by Hermitian function at each longitude). Mode 0 corresponds to the Yanai wave, while mode 1 to 4 indicates the Rossby waves with respective meridional structure.

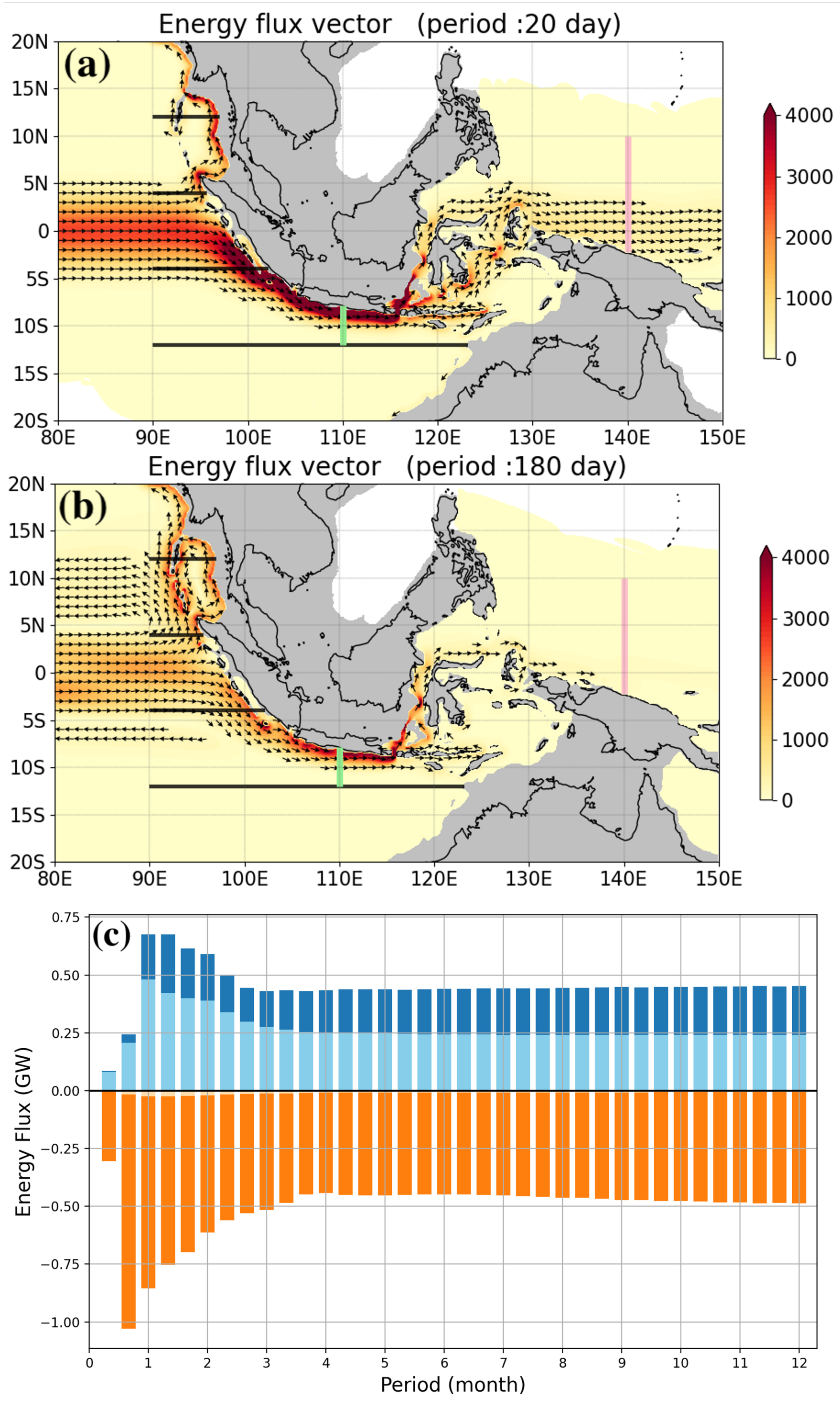

Figure 11. Horizontal distributions of the direction of energy flux vectors and magnitude of the energy flux for the forcing period of (a) 20 days and (b) 180 days. Only the vectors with their magnitude larger than 200 W m^{-1} are shown. (c) Northward energy fluxes across 4°N(*blue*), 4°S(*orange*), 12°N(*light blue*) and 12°S(*pale orange*) between 90°E and the eastern boundary coast of the Indian Ocean for each forcing period. The sections calculating the energy fluxes are shown with black lines. Negative values indicate southward energy fluxes.

ergy across 4°N peaks at about a period of one month, consistent with the observed short-period westward-propagating Rossby waves near 5°N (Chen et al., 2017).

Unlike the low frequency case, when the high frequency Kelvin wave excited in the equatorial Indian Ocean reaches the eastern boundary, more energy is distributed to the south, and the distribution ratio to the south increases with reduction of the frequency. This asymmetric characteristic of the north-south distribution for the short wavelength waves may be caused by the absence of westward reflecting Rossby waves at high frequencies (Fig. 11a) and also affected by the inclination of the eastern boundary of the Indian Ocean from the northsouth direction. This result suggests that when high frequency Kelvin wave reaches the inclined eastern boundary, more wave energy is distributed to the side where the boundary extends further east.

4.2 Energy flux pathways within the archipelago

The wave energy flux vectors in the Indonesian archipelago for the Indian experiments are shown in Fig. 12. An important common feature in all the results of these experiments with various forcing periods is that most of the incident energy enters the Indonesian archipelago through the Lombok Strait and then, flows into the western Pacific via the Makassar Strait. This waveguide is consistent with the route of wave signal predicted by Clarke and Liu (1994), suggested from observed data by Sprintall et al. (2000) and Pujiana et al. (2013), for example, and simulated in numerical models of Syamsudin et al. (2004), Schiller et al. (2010) and Yuan et al. (2018), for example. It is confirmed for the first time with direct estimation of the energy fluxes that the same routes can also be seen as the dominant energy pathways.

As in the case of the Pacific experiments, the results of Indian experiments demonstrate different characteristics between the low and high frequency cases. For the low frequency case, the Kelvin wave signals enter the Indonesian archipelago mainly via the Lombok Strait and slightly via the Ombai Strait. The energy entered the Indonesian seas via the Ombai Strait propagates westward along the northern coasts of the Lesser Sunda Islands around 8°S and merges with energy from Lombok Strait (see Fig. 12c).

On the other hand, in the high frequency case, there appears a new route passing through the Indonesian seas from the Lombok Strait to the Pacific Ocean. The wave energy coming into the archipelago via the Lombok Strait tends to follow the northward wave guide through the Makassar Strait. However, in the high frequency case (Fig. 12a), a part of this northward energy separates from the northward waveguide and propagates northeastward along the coast of Sulawesi Island and through the Molucca or Halmahera Seas to reach the Pacific Ocean. The energy fluxes along this additional waveguide decrease with increasing period, probably due to excitation of the Rossby waves, which transport the energy westward in the Flores Sea to the Makassar Strait at sufficiently long period. In addition, the westward energy propagation from the Ombai Strait is not as strong as the low frequency case, although the wave energy entering the Indonesian archipelago through the Ombai Strait is larger in the high frequency case compared to the low frequency case.

From the above results, two major wave energy pathways from the Indian to the Pacific Oceans can be found:

1. The wave propagates northward through the Lombok and Makassar Straits and then across the Celebes Sea to the Pacific Ocean,
2. After passing through the Lombok Strait, the wave propagates northeastward through the Flores Sea, and then reaches the Pacific Ocean via the Banda Sea and the Molucca or Halmahera Seas.

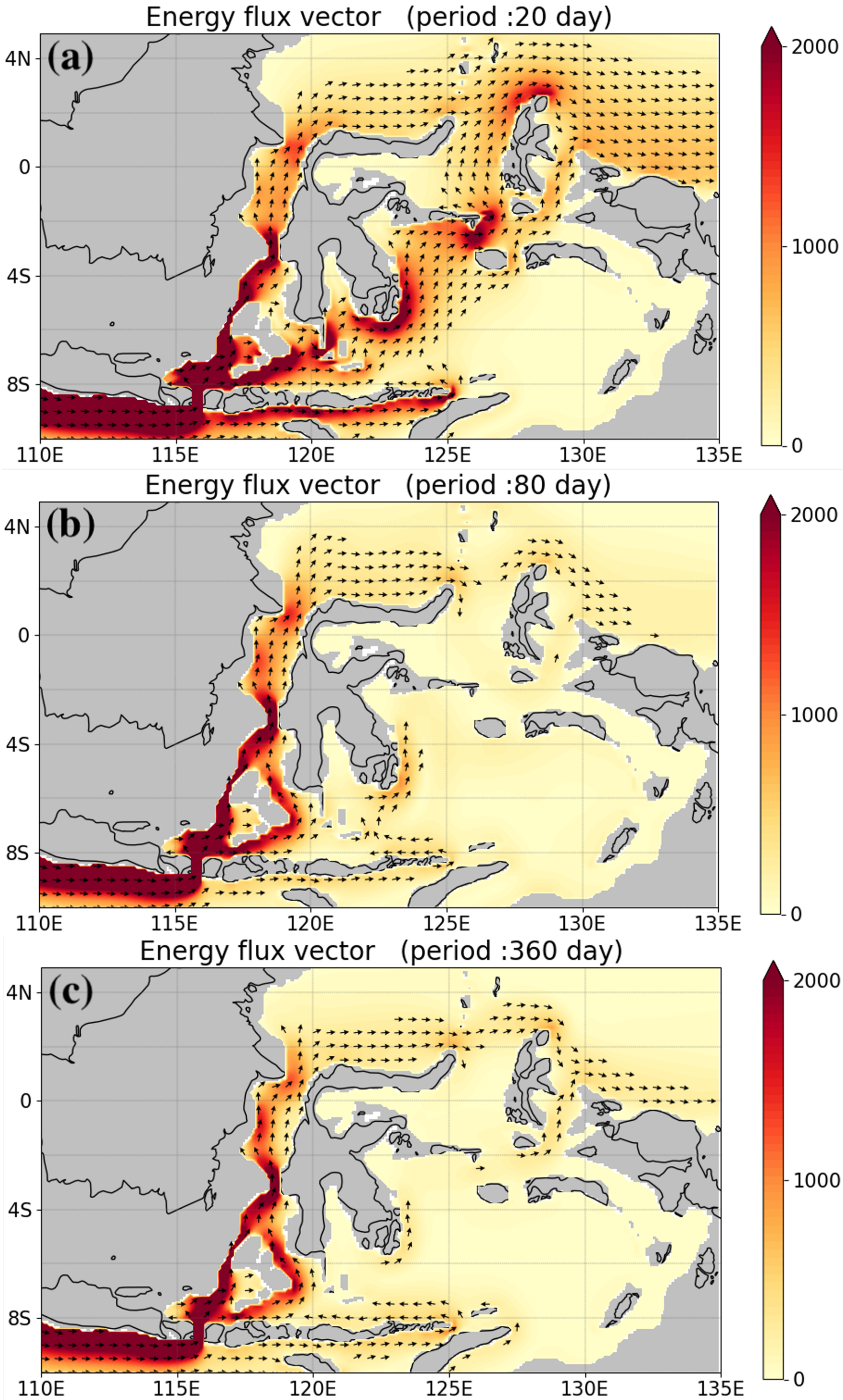

Figure 12. Horizontal distributions of the direction of energy flux vectors and magnitude of the energy flux within the Indonesian archipelago for the forcing period of (a) 20 days (b) 80 days, and (c) 360 days. Only the vectors with their magnitude larger than 200 W m^{-1} are shown.

The former pathway is found in all the experiments with various forcing periods. In contrast, the latter is found only in the experiments with the period of zonal wind forcing shorter than 2 months.

Theoretical and observational studies have reported that the coastal Kelvin waves propagating along the southern cost of Java Island can reach the Ombai Strait and that the associated wave energy enters the Indonesian archipelago through the Ombai Strait, as well as the Lombok Strait (Sprintall et al., 2000; Durland & Qiu, 2003; Syamsudin et al., 2004). It is noted that, in the present study, about 65% of the incoming wave energy passes through the Lombok Strait into the Indonesian archipelago except for the case with 10-day period forcing (not shown). This value is in good agreement with the results of Syamsudin et al. (2004), indicating $55.6 \pm 13.9\%$ from the altimeter data and 65% from the model designed for the first baroclinic mode waves. In the case of 10day period forcing, only about 30% of the incoming energy passes through the Lombok Strait, which may be due to the strong energy dissipation caused by short wavelength.

4.3 Energy transmission rate

The differences in the properties of short-period and long-period waves also appear in the wave energy transmission rate. Fig. 13 shows the incoming wave energy from Indian Ocean, E_{IO}, defined as the eastward energy flux across 110°E between 12°S and southern coast of Java Island (green line in Fig. 11a), the wave energy reaching the Pacific Ocean, E_{PA}, defined as the eastward energy flux across 140°E between 10°N and the northern coast of New Guinea Island (pink line in Fig. 11a), and transmission rate, $E_{\mathrm{PA}}/E_{\mathrm{IO}}$, for various period of the incoming waves. It is clearly shown that E_{IO} decreases as the forcing period increases, except for the shortest period of 10 days. This is consistent with the meridional energy partition of the equatorial Kelvin wave off the coast of Sumatra Island shown in Fig. 11c. The energy transmitted to the Pacific Ocean, E_{PA}, also decreases as the period increases, but is almost constant for the periods longer than 3 months. Thus, the transmission rate increases sightly with the forcing period for the periods longer than 3 months. In the experiments with the shorter period forcing, the transmission rate has a minimum value of about 12% at the 50-day period, while the maximum of about 27% appears at the 20-day period. It can be said that this maximum transmission rate corresponds to the existence of the additional pathway for the shorter forcing period shown in Fig. 12a.

The energy transmission rate at high frequency in Fig. 13 does not agree with the result of one-dimensional wave interference problem through an ideal strait by Durland and Qiu (2003). They showed that the energy transmission rate increases monotonically as the wave period increases in a narrow channel-like passage similar to the Lombok Strait. In fact, the transmission rate only for the Lombok Strait in this study does not increase with the period either. However, because the obtained energy fluxes are time-averaged over one forcing period, the energy fluxes through the Lombok Strait are caused by superposition of the northward propagating energy directly from the Indian Ocean and the southward propagating energy returning to the Indian Ocean, which enters the Indonesian archipelago through the Ombai Strait or the Timor Sea and propagates back as the coastal Kelvin waves. Therefore, our results do not represent a pure amount of the northward energy propagation through the Lombok Strait. In other words, the northward energy propagation through the Lombok Strait in the realistic condition may be rather different from the idealized case shown in Durland and Qiu (2003). In addition, the resolution of our experiment, 1/10 degrees, may be too coarse to consider the very narrow straits.

Since it is difficult to discuss the transmission rate by focusing on particular passages, for example via the Lombok Strait as mentioned above, we consider the energy which goes across the equator to the north through the Makassar Strait (E_{Makassar}), the

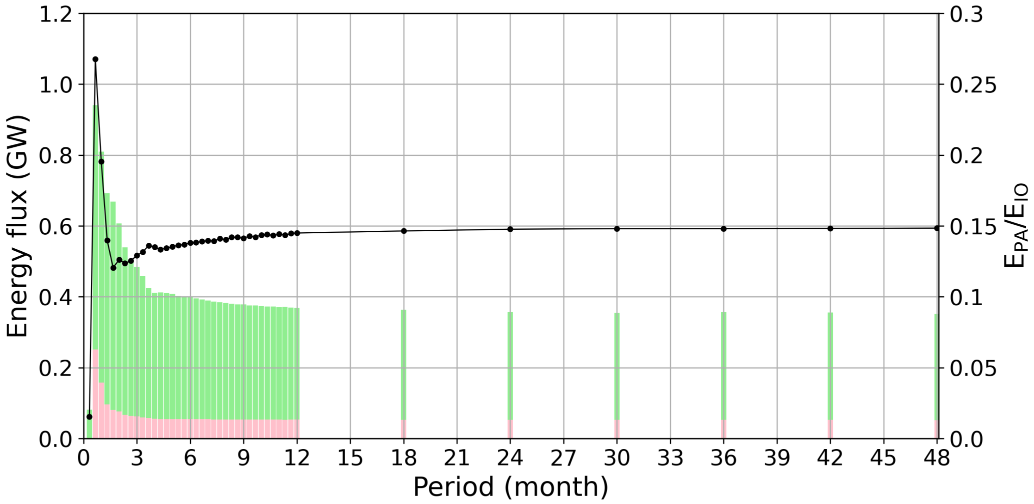

Figure 13. Incoming wave energy flux from the Indian Ocean $E_{\rm IO}$(*green*), the wave energy reaching the Pacific Ocean $E_{\rm PA}$ (*pink*), and transmission rate $E_{\rm PA}/E_{\rm IO}$ (*solid line*) as a function of the forcing period.

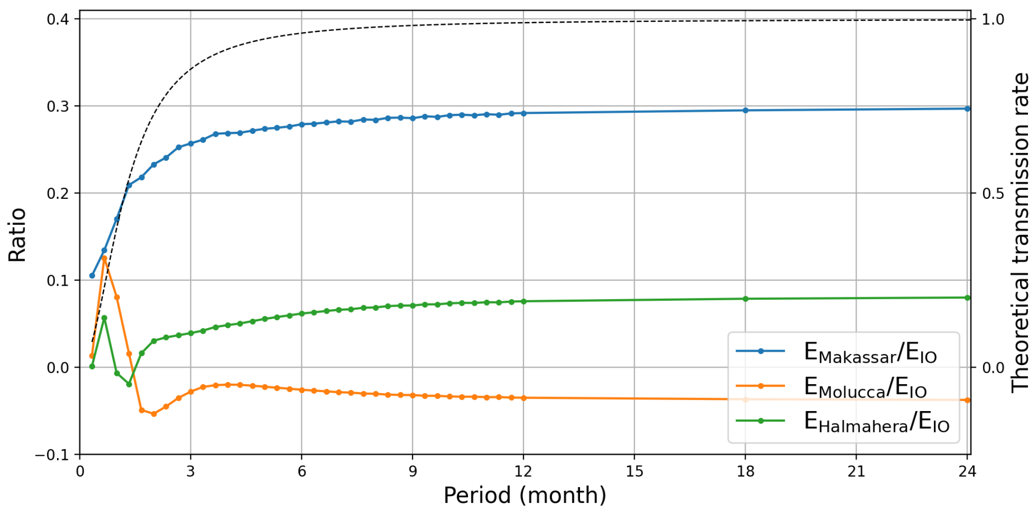

Figure 14. The ratio of the northward energy flux across the equator through the Makassar Strait ($E_{\rm Makassar}$), the Molucca Sea ($E_{\rm Molucca}$), and the Halmahera Sea ($E_{\rm Halmahera}$) relative to the incoming wave energy from the Indian Ocean ($E_{\rm IO}$) as a function of the forcing period (left axis). Theoretical wave energy transmission rates for each Kelvin wave period based on the Kelvin wave transmission theory (Durland & Qiu, 2003) (dashed line, right axis). The theoretical transmission rates are calculated for the narrowest part of the Makassar strait at 3°N, 50 km wide and 100 km long.

Molucca Sea (E_{Molucca}) and the Halmahera Sea ($E_{\mathrm{Halmahera}}$). It is noted that the coastal Kelvin waves trapped around the islands, which are superimposed on the pure incoming waves, cannot cross the equator. Fig. 14 shows the transmission ratio of E_{Makassar}, E_{Molucca} and $E_{\mathrm{Halmahera}}$ to the incoming wave energy, propagating eastward off the southern coast of Java Island (E_{IO}). The transmission rate of the Makassar Strait increases as the wave period increases in the shorter periods and is almost constant in the longer periods. The Kelvin waves approaching to the Makassar Strait are not expected to pass smoothly, because the width of the strait at the narrowest part of the Makassar Strait is narrower than 1/5 of the deformation radius. Fig. 14 also shows the theoretical energy transmission rate through the Makassar Strait calculated based on the Kelvin wave transmission theory through the strait narrower than the deformation radius (Durland & Qiu, 2003). The energy transmission rate becomes smaller for shorter period Kelvin waves because the phase of the incoming Kelvin waves changes before the adjustment in the strait is completed. Comparing the theory (dashed line Fig. 14) and our results (blue line in Fig. 14), the energy transmission rate is almost constant for sufficiently long period in both cases. However, the constant values are very different: it's almost 1 in the theory while it's about 0.3 in the model results. This discrepancy may be due to the inability to accurately estimate the incoming energy into the Makassar Strait for the model result and to the lack of the viscous effect in the theory of Durland and Qiu (2003) as pointed out by Johnson and Garrett (2006). Nevertheless, their dependencies on the incoming wave period show the similar tendency. Thus, it is reasonable to consider that the smaller energy transmission rate for the shorter period Kelvin waves in the model is due to incomplete adjustment in the strait with the faster phase change of the incoming Kelvin waves, as discussed in Durland and Qiu (2003).

Unlike the Makassar Strait, the transmission rates of the Molucca Sea and Halmahera Sea do not increase with increasing the period and have a maximum and a negative minimum in the periods shorter than 3 months. This peculiar behavior may be related to the complicated wave propagation around the Halmahera Island associated with the additional eastern pathway of the wave energy within the Indonesian archipelago. Fig. 14 also shows that the transmission rates of the Molucca Sea and Halmahera Sea are much smaller than that of the Makassar Strait in all the periods, suggesting the main route of the wave energy through the Makassar Strait. It is interesting to note that the sum of the transmission rate for the three passages in Fig. 14 is far less than 1, which seems to be caused by the effect of energy dissipation. Horizontal distributions of the energy dissipation rate indicates that the strong energy dissipation appears along the major route of the energy flux from the Lombok Strait to the Makassar Strait (not shown). The dissipation rate is larger in the west at each latitude within the archipelago, suggesting the importance of the western boundary layer as in the results of the Pacific experiments.

5 Summary and Discussion

The detailed pathways of the equatorial wave energy through the Indonesian archipelago and the processes responsible for the formation of the pathways are investigated using a 1.5-layer reduced gravity model, for the incoming waves both from the Pacific Ocean and from the Indian Ocean. The energy transmission rates between the two basins are also quantitatively explored for a wide range of the forcing period. In order to evaluate the wave energy flux in the equatorial region, the formulation proposed by Aiki et al. (2017) is utilized. This energy flux analysis scheme has enabled us to perform a unified treatment of the equatorial and mid-latitude Rossby waves and the equatorial and coastal Kelvin waves. It can also show directly how the energy of incoming waves from the Pacific Ocean reaches the Indian Ocean and vice versa.

For the case of incoming Rossby waves from the Pacific Ocean, most of the wave energy propagates southward through the Halmahera Sea and reaches the Indian Ocean via the Banda and Timor Seas. It turns out that the wave energy propagating around the island chain in the Banda Sea cancels the southward energy flux along the easternmost route and has the main pathway shifted to the western side of the island chain. Another pathway to the Indian Ocean via the Makassar Strait also shows significant magnitude of energy flux, but the energy entering the Indonesian Seas through the Makassar Strait is about a quarter of the one through the Halmahera Sea. This wave energy flux distribution is different from the transport distribution of the ITF mean flow which enters the Indonesian archipelago mainly through the Makassar Strait (Gordon & Fine, 1996; Gordon, 2005). Therefore, it is suggested that not only the western pathway via the Makassar Strait but also the eastern pathway via the Banda Sea should be considered to investigate the impacts of the variabilities in the tropical Pacific Ocean on the Indonesian archipelago.

The energy budget analysis indicates that both the transmitted and reflected wave energy decreases significantly for the wave period shorter than 1.5 years, which is mainly due to the increase in energy dissipation along the northern coast of New Guinea. The different characteristics of the energy propagation for the shorter period waves may be related to the geometry of the western boundary of the equatorial Pacific Ocean. The zonal wavelength of the first meridional mode equatorial Rossby wave at the 1.5-year period is about 40,000 km, which is equivalent to about two times the zonal width of New Guinea. For this reason, the meridional wall approximation adopted by Clarke (1991) may be appropriate when the period of incoming Rossby wave is longer than 1.5-year.

The inclination of the New Guinea coast also affects mass flux along the coast. The reflection of the equatorial Rossby waves at the inclined western boundary has already investigated by considering mass flux normal to the coastline (Cane & Gent, 1984; McCalpin, 1987). In these studies, the reflected short Rossby wave merely redistributes mass along the coastline, and the incoming mass flux of the incident Rossby wave and the outgoing mass flux of the reflected Kelvin wave are balanced. When the western boundary is inclined, however, the total incoming mass flux normal to the coastline decreases because the phase difference along the boundary induces incoming and outgoing mass fluxes simultaneously. This decrease of incoming mass flux becomes more important as the wavelength of the incident wave becomes shorter. Thus, the decrease of reflection rate with decreasing wave period shown in this study (see Fig. 7) is partly due to the change in the total mass flux balance along the western boundary. However, the reduction of reflection rate in the present study is more rapid than that explained by the mass flux balance only, and this difference may be explained by the energy dissipation in the boundary layer. The phase shift of the incoming mass flux along the western boundary causes the strong boundary flow to redistribute mass within the boundary layer. This boundary flow forms the strong horizontal velocity shear, which induces the large energy dissipation. Therefore, the reduction of reflection rate in the shorter period cases shown in Fig. 7 may be due to the change in the mass flux balance at the western boundary and to the energy dissipation associated with the enhanced boundary flow. Furthermore, our simple simulations show that incoming semiannual Rossby waves can excite intraseasonal Yanai wave at tilted western boundary (see Fig. 9b). This result suggests that the intraseasonal Yanai waves near the western boundary are excited not only by direct wind forcing or instability as suggested by previous studies (e.g. Chatterjee et al., 2013), but also by reflection of the long Rossby waves with longer periods.

It is worth mentioning that additional experiments with advective terms show similar results with about 2% decrease in the transmission rate and about 2% increase in the reflection rate (not shown), therefore, nonlinear effects may have some influences on the Rossby wave reflection on the western boundary as suggested by Yuan and Han (2006); Yuan et al. (2019) and the wave intrusion into the Indonesian archipelago. Despite the decrease of wave energy entering the Indonesian archipelago, the behaviors of waves in the archipelago are similar to those in the linear experiments. It is also noted that the nonlinear experiments in the present study do not include ITF like mean flow, thus no wave-mean flow interaction is taken into account.

In the case of the Kelvin waves propagating from the equatorial Indian Ocean, about half of the incident wave energy onto the eastern boundary for the period longer than one month is distributed to the south off the western coast of Sumatra Island and continues propagating eastward along the Sumatra and Java Islands as the coastal Kelvin waves. When the incoming wave period is shorter than one month, most of the wave energy is distributed to the south. The eastward coastal Kelvin waves enter the Indonesian Seas through the Lombok and Ombai Straits and propagate northward through the Makassar Strait to reach the western Pacific. Another pathway to the western Pacific via the Banda Sea appears clearly only when the incoming wave period is shorter than 2 months. The energy budget analysis indicates that about 15% of the incoming wave energy reaches the western Pacific for the incoming wave period longer than 1 year. The transmission rate also has a peak at 20-day period with a value of about 27%, corresponding to the existence of the additional pathway. Considering such intraseasonal waves is important because observed transport signal at ITF outflow passages suggest the Kelvin waves forced by periodic winds with period of 28-46 days (Drushka et al., 2010).

The shorter period Kelvin waves from the Indian Ocean can enter the Indonesian archipelago, much easier compared to the Rossby waves from the Pacific Ocean, and the transparency of narrow straits play an important role on this difference. The straits narrower than the deformation radius, such as the Lombok and Makassar Straits, tend to suppress the transmission of the short-period waves (Durland & Qiu, 2003). Because this suppression depends strongly on the ratio of deformation radius to the width of passage, the location of the strait is important. The Makassar Strait is located at a lower latitude than the Lombok Strait, thereby the deformation radius becomes larger at the Makassar Strait. When the incoming Kelvin waves with a period of about one month enter the Indonesian archipelago, much energy can propagate through the Lombok Strait, but not through the Makassar Strait, where the strong energy dissipation occurs instead. This may be the reason for the wave energy to reach the Pacific via the Banda Sea for the period shorter than one month.

Most of the incident wave energy enters the Indonesian archipelago through the Lombok Strait in the present study. The wave signals from the equatorial Indian Ocean, however, have also been observed in the Ombai Strait (Molcard et al., 2001; Potemra et al., 2002; Sprintall et al., 2009; Drushka et al., 2010). Drushka et al. (2010) suggest that the Kelvin wave signals in the Ombai Strait is due to the downward propagation that prevent the incoming Kelvin wave from passing through the shallow Lombok Strait. The 1.5-layer reduced gravity model does not include such vertical process, thus, may not be sufficient for the realistic representations of the Kelvin wave penetration into the archipelago. However, the high transmission rates and the additional eastern energy pathway for intraseasonal waves are still apparent in sensitivity experiments without the Lombok Strait (not shown).

Although only 10% of the incoming wave energy from the Pacific Ocean reaches the southeastern Indian Ocean, the wave signals from the Pacific Ocean certainly affect the interannual variability in the Indian Ocean, such as the Leeuwin Current (Feng et al., 2003) and the Ningaloo Niño (Kataoka et al., 2014). On the other hand, about 10% of the incoming wave energy from the Indian Ocean reaches the Pacific Ocean in the present study. However, the ocean waves from the Indian Ocean have not been observed in the western Pacific Ocean. These differences of ocean waves in reality may be due to the difference in period of the dominant variations or intensities of the forcing between the Pacific and Indian Oceans, which would be the important questions for future works.

Appendix A Formation of Energy Flux

Derivation of a new formulation of the energy flux proposed by Aiki et al. (2017) (hereafter AGC17) is briefly shown here. Following AGC17, we assume linear waves in the absence of a mean flow on an equatorial β-plane. Then, the linear shallow water equations are nondimensionalized, with the time scale of $1/\sqrt{c\beta}$ and length scale of $\sqrt{c/\beta}$, as:

$$\begin{aligned} &\tfrac{\partial u}{\partial t} - yv + \tfrac{\partial p}{\partial x} = 0 \\ &\tfrac{\partial v}{\partial t} + yu + \tfrac{\partial p}{\partial y} = 0 \\ &\tfrac{\partial p}{\partial t} + \tfrac{\partial u}{\partial x} + \tfrac{\partial v}{\partial y} = 0 \end{aligned} \tag{A1}$$

where p indicates pressure. Manipulation of the equations A1 yields the wave energy equation

$$\frac{\partial}{\partial t}(u^2 + v^2 + p^2)/2 + \nabla \cdot \langle up, vp \rangle = 0 \tag{A2}$$

where $\langle\cdot\rangle$ means a horizontal vector. According to this energy equation A2, the divergence of pressure flux, $\nabla\cdot\langle up, vp\rangle$, accurately represent the time rate of energy change at a particular location. However, the pressure flux itself does not always point in the direction of the group velocity vector, i.e.

$$\langle up, vp \rangle \neq \left\langle \frac{\partial \omega}{\partial k}, \frac{\partial \omega}{\partial l} \right\rangle (u^2 + v^2 + p^2)/2 \tag{A3}$$

where ω is wave frequency, k and l are zonal and meridional wavenumber respectively. In mid-latitudes, this problem can be avoided by taking into account the pressure flux associated with geostrophic flows Orlanski and Sheldon (1993). In contrast, in equatorial regions, we cannot consider geostrophic flows. Therefore, another diagnostic quantity that represents the difference between the two sides of equation A3 is required to evaluate the energy flux.

(Matsuno, 1966) has derived a solution to equation A1 on the equatorial β-plane, which is shown as

$$\begin{aligned} v &= A\cos\theta \exp(-y^2/2) H^{(n)} \\ u &= (\omega y v_\theta - k v_{y\theta})/(\omega^2 - k^2) \\ p &= (k y v_\theta - \omega v_{y\theta})/(\omega^2 - k^2) \end{aligned} \tag{A4}$$

where A is wave amplitude, $H^{(n)}$ is the Helmite polynominal with n being the meridional mode number, θ is wave phase $(kx-\omega t)$. The subscript represents partial differentiation. By using the solutions A4, phase averaged zonal pressure flux can be written as

$$\overline{up} = \overline{vv}(2\omega k + 1)/[2(\omega^2 - k^2)] + [\overline{v_y v}(2\omega k) - y\overline{vv}(\omega^2 + k^2)]_y/[2(\omega^2 - k^2)^2]$$

where overbar denotes the phase average. In the same way, the wave energy can be decomposed into two parts,

$$\left(\overline{u^2 + v^2 + p^2}\right)/2 = \overline{vv}(2\omega^2 + k/\omega)/[2(\omega^2 - k^2)] + [\overline{v_y v}(\omega^2 + k^2) - y\overline{vv}(2k\omega)]_y/[2(\omega^2 - k^2)^2]$$

Then we can obtain an analytical expression for difference between the right and left sides of A3 to yield

$$(\partial\omega/\partial k)(\overline{u^2 + v^2 + p^2})/2 - \overline{up} = \frac{-(\overline{pv_\theta})_y - (2\overline{u_{tt}v_\theta})_y}{2k(1 + 2\omega^3/k)}$$

Finally, the right hand side of the equation A3, i.e. zonal component of the group velocity times wave energy can be rewritten in phase averaged form:

$$(\partial\omega/\partial k)(\overline{u^2 + v^2 + p^2})/2 = \overline{up} + (\overline{p\varphi}/2 + \overline{u_{tt}\varphi})_y$$

$$\varphi \equiv -v_\theta/(k+2\omega^3) \tag{A5}$$

Meridional component of the group velocity times wave energy can also be derived in the same way. Furthermore, the definition of φ, the equation A5, can be written as

$$\nabla^2\varphi - y^2\varphi - 3\varphi_{tt} = -v_\theta/\omega = q$$

where q is the Ertel's potential vorticity. Therefore the scalar quantity φ can be estimated without using Fourier analysis, and then we can diagnostically estimate energy flux vector even with coastal boundaries. Moreover the scalar quantity φ is also applicable to mid-latitude waves. Thus, we can trace wave propagations at all latitude with coastal boundary by using the AGC17 scheme.

In the present study, we use simplified energy flux, called as level-2 flux in AGC17, in order to reduce the computational cost. Note that the level-2 flux provides an approximate expression for energy flux based on the group velocity of both low- and high- frequency equatorial waves. To calculate the level-2 energy flux vector of AGC17 scheme, the following approximated inverse problem in dimensionalized form is solved numerically, using results obtained during the last forcing period of our simulations:

$$\nabla^2\varphi^{app} - (f/c)^2\,\varphi^{app} = q \tag{A6}$$

where $q = \frac{\partial v}{\partial x} - \frac{\partial u}{\partial y} - (f/c^2)p$ is the linearized Ertel's potential vorticity and p indicates pressure. Then, using φ^{app} obtained by soliving the equation A6, we calculate the level-2 energy flux vector in the dimensionalized form:

$$\overline{\mathbf{V}p} + \nabla \times (\overline{p\varphi^{app}})/2$$

where $\mathbf{V}$ is horizontal velocity vector and overbar denotes the phase average.

Open Research Section

ETOPO1 1 Arc-Minute Global Relief Model data are provided by the National Oceanic and Atmospheric Administration at https://www.ngdc.noaa.gov/mgg/global/.

References

Aiki, H., Greatbatch, R. J., & Claus, M. (2017). Towards a seamlessly diagnosable expression for the energy flux associated with both equatorial and mid-latitude waves. *Progress in Earth and Planetary Science*, *4*(1), 1–18.

Amante, C., & Eakins, B. W. (2009). Etopo1 arc-minute global relief model: procedures, data sources and analysis.

Boulanger, J.-P., & Fu, L.-L. (1996). Evidence of boundary reflection of kelvin and first-mode rossby waves from topex/poseidon sea level data. *Journal of Geophysical Research: Oceans*, *101*(C7), 16361–16371.

Boulanger, J.-P., & Menkes, C. (1995). Propagation and reflection of long equatorial waves in the pacific ocean during the 1992–1993 el nino. *Journal of Geophysical Research: Oceans*, *100*(C12), 25041–25059.

Boulanger, J.-P., & Menkès, C. (1999). Long equatorial wave reflection in the pacific ocean from topex/poseidon data during the 1992–1998 period. *Climate dynamics*, *15*(3), 205–225.

Busalacchi, A. J., McPhaden, M. J., & Picaut, J. (1994). Variability in equatorial pacific sea surface topography during the verification phase of the topex/poseidon mission. *Journal of Geophysical Research: Oceans*, *99*(C12), 24725–24738.

Cane, M. A., & Gent, P. R. (1984). Reflection of low-frequency equatorial waves at arbitrary western boundaries. *Journal of Marine Research*, *42*(3), 487–502.
Chatterjee, A., Shankar, D., McCreary Jr, J., & Vinayachandran, P. (2013). Yanai waves in the western equatorial indian ocean. *Journal of Geophysical Research: Oceans*, *118*(3), 1556–1570.
Chen, G., Han, W., Li, Y., McPhaden, M. J., Chen, J., Wang, W., & Wang, D. (2017). Strong intraseasonal variability of meridional currents near 5° n in the eastern indian ocean: Characteristics and causes. *Journal of Physical Oceanography*, *47*(5), 979–998.
Clarke, A. J. (1991). On the reflection and transmission of low-frequency energy at the irregular western pacific ocean boundary. *Journal of Geophysical Research: Oceans*, *96*(S01), 3289–3305.
Clarke, A. J., & Liu, X. (1994). Interannual sea level in the northern and eastern indian ocean. *Journal of Physical Oceanography*, *24*(6), 1224–1235.
Drushka, K., Sprintall, J., Gille, S. T., & Brodjonegoro, I. (2010). Vertical structure of kelvin waves in the indonesian throughflow exit passages. *Journal of Physical Oceanography*, *40*(9), 1965–1987.
Du Penhoat, Y., & Cane, M. A. (1991). Effect of low-latitude western boundary gaps on the reflection of equatorial motions. *Journal of Geophysical Research: Oceans*, *96*(S01), 3307–3322.
Durland, T. S., & Qiu, B. (2003). Transmission of subinertial kelvin waves through a strait. *Journal of Physical Oceanography*, *33*(7), 1337–1350.
Feng, M., Meyers, G., Pearce, A., & Wijffels, S. (2003). Annual and interannual variations of the leeuwin current at 32 s. *Journal of Geophysical Research: Oceans*, *108*(C11).
Gordon, A. L. (1986). Interocean exchange of thermocline water. *Journal of Geophysical Research: Oceans*, *91*(C4), 5037–5046.
Gordon, A. L. (2005). Oceanography of the indonesian seas and their throughflow. *Oceanography*, *18*(4), 14–27.
Gordon, A. L., & Fine, R. A. (1996). Pathways of water between the pacific and indian oceans in the indonesian seas. *Nature*, *379*(6561), 146–149.
Gordon, A. L., Susanto, R. D., & Ffield, A. (1999). Throughflow within makassar strait. *Geophysical Research Letters*, *26*(21), 3325–3328.
Hendon, H. H., Liebmann, B., & Glick, J. D. (1998). Oceanic kelvin waves and the madden–julian oscillation. *Journal of the Atmospheric Sciences*, *55*(1), 88–101.
Johnson, H. L., & Garrett, C. (2006). What fraction of a kelvin wave incident on a narrow strait is transmitted? *Journal of Physical Oceanography*, *36*(5), 945–954.
Kataoka, T., Tozuka, T., Behera, S., & Yamagata, T. (2014). On the ningaloo niño/niña. *Climate dynamics*, *43*(5-6), 1463–1482.
Li, J., & Clarke, A. J. (2004). Coastline direction, interannual flow, and the strong el niño currents along australia's nearly zonal southern coast. *Journal of Physical Oceanography*, *34*(11), 2373–2381.
Li, X., Yuan, D., Wang, Z., Li, Y., Corvianawatie, C., Surinati, D., … others (2020). Moored observations of transport and variability of halmahera sea currents. *Journal of Physical Oceanography*, *50*(2), 471–488.
Li, Z., & Aiki, H. (2020). The life cycle of annual waves in the indian ocean as identified by seamless diagnosis of the energy flux. *Geophysical Research Letters*, *47*(2), e2019GL085670.
Madden, R. A., & Julian, P. R. (1994). Observations of the 40–50-day tropical oscillation—a review. *Monthly weather review*, *122*(5), 814–837.
Matsuno, T. (1966). Quasi-geostrophic motions in the equatorial area. *Journal of the Meteorological Society of Japan. Ser. II*, *44*(1), 25–43.
McCalpin, J. D. (1987). A note on the reflection of low-frequency equatorial rossby

waves from realistic western boundaries. *Journal of Physical Oceanography*, *17*(11), 1944–1949.
Molcard, R., Fieux, M., & Syamsudin, F. (2001). The throughflow within ombai strait. *Deep Sea Research Part I: Oceanographic Research Papers*, *48*(5), 1237–1253.
Murtugudde, R., Busalacchi, A. J., & Beauchamp, J. (1998). Seasonal-to-interannual effects of the indonesian throughflow on the tropical indo-pacific basin. *Journal of Geophysical Research: Oceans*, *103*(C10), 21425–21441.
Orlanski, I., & Sheldon, J. (1993). A case of downstream baroclinic development over western north america. *Monthly Weather Review*, *121*(11), 2929–2950.
Potemra, J. T. (2001). Contribution of equatorial pacific winds to southern tropical indian ocean rossby waves. *Journal of Geophysical Research: Oceans*, *106*(C2), 2407–2422.
Potemra, J. T., Hautala, S. L., Sprintall, J., & Pandoe, W. (2002). Interaction between the indonesian seas and the indian ocean in observations and numerical models. *Journal of Physical Oceanography*, *32*(6), 1838–1854.
Pujiana, K., Gordon, A. L., & Sprintall, J. (2013). Intraseasonal kelvin wave in makassar strait. *Journal of Geophysical Research: Oceans*, *118*(4), 2023–2034.
Qiu, B., Mao, M., & Kashino, Y. (1999). Intraseasonal variability in the indo–pacific throughflow and the regions surrounding the indonesian seas. *Journal of Physical Oceanography*, *29*(7), 1599–1618.
Qu, T., Gan, J., Ishida, A., Kashino, Y., & Tozuka, T. (2008). Semiannual variation in the western tropical pacific ocean. *Geophysical Research Letters*, *35*(16).
Schiller, A., Wijffels, S., Sprintall, J., Molcard, R., & Oke, P. R. (2010). Pathways of intraseasonal variability in the indonesian throughflow region. *Dynamics of atmospheres and oceans*, *50*(2), 174–200.
Sloyan, B. M., & Rintoul, S. R. (2001). Circulation, renewal, and modification of antarctic mode and intermediate water. *Journal of Physical Oceanography*, *31*(4), 1005–1030.
Spall, M. A., & Pedlosky, J. (2005). Reflection and transmission of equatorial rossby waves. *Journal of Physical Oceanography*, *35*(3), 363–373.
Sprintall, J., Gordon, A. L., Murtugudde, R., & Susanto, R. D. (2000). A semiannual indian ocean forced kelvin wave observed in the indonesian seas in may 1997. *Journal of Geophysical Research: Oceans*, *105*(C7), 17217–17230.
Sprintall, J., Wijffels, S. E., Molcard, R., & Jaya, I. (2009). Direct estimates of the indonesian throughflow entering the indian ocean: 2004–2006. *Journal of Geophysical Research: Oceans*, *114*(C7).
Suarez, M. J., & Schopf, P. S. (1988). A delayed action oscillator for enso. *Journal of Atmospheric Sciences*, *45*(21), 3283–3287.
Syamsudin, F., Kaneko, A., & Haidvogel, D. B. (2004). Numerical and observational estimates of indian ocean kelvin wave intrusion into lombok strait. *Geophysical research letters*, *31*(24).
Wijffels, S., & Meyers, G. (2004). An intersection of oceanic waveguides: Variability in the indonesian throughflow region. *Journal of Physical Oceanography*, *34*(5), 1232–1253.
Wyrtki, K. (1987). Indonesian through flow and the associated pressure gradient. *Journal of Geophysical Research: Oceans*, *92*(C12), 12941–12946.
Yuan, D., & Han, W. (2006). Roles of equatorial waves and western boundary reflection in the seasonal circulation of the equatorial indian ocean. *Journal of Physical Oceanography*, *36*(5), 930–944.
Yuan, D., Hu, X., Xu, P., Zhao, X., Masumoto, Y., & Han, W. (2018). The iod-enso precursory teleconnection over the tropical indo-pacific ocean: dynamics and long-term trends under global warming. *Journal of Oceanology and Limnology*, *36*(1), 4–19.
Yuan, D., Song, X., Yang, Y., & Dewar, W. K. (2019). Dynamics of mesoscale ed-

dies interacting with a western boundary current flowing by a gap. *Journal of Geophysical Research: Oceans*, *124*(6), 4117–4132.

Zhang, C., Hendon, H. H., Kessler, W. S., & Rosati, A. J. (2001). A workshop on the mjo and enso. *Bulletin of the American Meteorological Society*, *82*(5), 971–976.